# The Chelyabinsk airburst : Implications for the Impact Hazard

P.G. Brown[1,2], J. D. Assink[3], L. Astiz[4], R. Blaauw[5], M.B. Boslough[6], J. Borovicka[7], N. Brachet[3], D. Brown[8], M. Campbell-Brown[1], L. Ceranna[9], W. Cooke[10], C. de Groot-Hedlin[4], D. Drob[11], W. Edwards[12], L.G. Evers[13,14], M. Garces[15], J. Gill[1], , M. Hedlin[4], A. Kingery[16], G. Laske[4], A. Le Pichon[3], P. Mialle[8], D.E. Moser[5], A. Saffer[10], E. Silber[1], P. Smets[13,14], R.E. Spalding[6], P. Spurny[7], E. Tagliaferri[17], D. Uren[1], R.J. Weryk[1], R. Whitaker[18], Z. Krzeminski[1]

[1]Dept. of Physics and Astronomy, University of Western Ontario, London, Ontario, N6A 3K7, Canada [2]Centre for Planetary Science and Exploration, University of Western Ontario, London, Ontario, N6A 5B7, Canada [3]CEA/DAM/DIF, F-91297 Arpajon, France [4]Laboratory for Atmospheric Acoustics, Institute of Geophysics and Planetary Physics, University of California, San Diego, La Jolla, California, USA [5]MITS/Dynetics Technical Services, NASA Marshall Space Flight Center, Huntsville, Alabama 35812, USA [6]Sandia National Laboratories, P. O. Box 5800, Albuquerque, New Mexico 87185, USA [7]Astronomical Institute, Academy of Sciences of the Czech Republic, CZ 251 65 Ondrejov, Czech Republic [8]International Data Center, Provisional Technical Secretariat, Comprehensive Test Ban Treaty Organization, P.O. Box 1200, A-1400 Vienna, Austria [9]Bundesanstalt für Geowissenschaften und Rohstoffe, Stilleweg 2, 30655 Hannover, Germany [10]Meteoroid Environments Office, EV44, Space Environment Team, Marshall Space Flight Center, Huntsville, Alabama, 35812 USA [11]Space Science Division, Naval Research Laboratory, 4555 Overlook Ave., Washington, D.C., 20375, USA [12]Natural Resources Canada, Canadian Hazard Information Service, 7 Observatory Crescent, Ottawa, Ontario, K1A 0Y3, Canada [13]Seismology Division, Royal Netherlands Meteorological Institute, Wilhelminalaan 10, 3732 GK De Bilt, the Netherlands [14]Department of Geoscience and Engineering, Faculty of Civil Engineering and Geosciences, Delft University of Technology, Stevinweg 1,2628 CN Delft, the Netherlands.[15]Infrasound Laboratory, University of Hawaii, Manoa 73-4460 Queen Kaahumanu Hwy., #119 Kailua-Kona, Hawaii 96740-2638 [16]ERC Incorporated/Jacobs ESSSA Group, NASA Marshall Space Flight Center, Huntsville, Alabama 35812 [17]ET Space Systems, 5990 Worth Way, Camarillo,

California 93012, USA [18]Los Alamos National Laboratory, EES-17 MS F665, P.O. Box 1663 Los Alamos, New Mexico 87545, USA

**The recent discovery of most large (>1 km) near Earth asteroids (NEAs) and recognition of the greater damage potential from airbursts (large fireballs)[1], has shifted an increasing portion of the remaining impact risk (which depends on both the number of impactors and their individual effects) to smaller objects[2]. At the threshold impactor size where the atmosphere absorbs sufficient energy to prevent a ground impact, the primary damage mode is believed to be from the airburst shock wave[3], but this is uncertain due to lack of observations[4,5]. Here we report on damage from the ~500 ± 100 kiloton airburst of a ~19 (17-20) m diameter asteroid SE of Chelyabinsk, Russia on Feb 15, 2013. We show that a widely referenced method[4,5,6] of estimating airburst damage does not reproduce observations while nuclear weapons effects relations[7] often used with this technique overestimates blast damage. This suggests that earlier damage estimates[5,6] near the threshold are too high. From a global survey of kiloton and larger airbursts (including Chelyabinsk) we find that the number of impactors may be an order of magnitude higher in the range of tens of meters in diameter as compared to other techniques[8,9], suggesting a non-equilibrium in the NEA population for 10 - 50m objects and shifting more of the residual impact risk to these sizes.**

The Chelyabinsk fireball[10] was observed globally by multiple instruments, including infrasound, seismic, US government sensors and over 400 video cameras at ranges up to 700 km. The resulting airblast shattered thousands of windows in urban Chelyabinsk, with flying glass injuring many residents.

Data from US Government sensors timed the peak brightness to 03:20:32.2 UTC, Feb 15, 2013 with an integrated radiated energy of $3.75\times10^{14}$ J and a peak brightness of $2.7\times10^{13}$ W/sr. These values correspond to an estimated energy equivalent of ~530 kt TNT. The peak brightness was equivalent to an absolute astronomical magnitude of -28 (referenced to a range of 100 km) in the silicon bandpass, making the airburst appear 30 times brighter than the sun to an observer directly under this point. The fireball lightcurve has been reconstructed by considering the measured light production from several video records (see Supplementary Information for details) as shown in Figure 1. Of note is the fact that point-like models[4,5,6] of bolide energy disruption, which treat the impactor as a strengthless, liquid-like material, predict half energy deposition in a <2 km heights range for impacts as shallow (17 degrees from the horizontal)[10] as Chelyabinsk, less than 1/3 the observed value. These models[4,5,6] also underestimate the lateral fragmentation speeds observed in the airburst[10]. Airburst energy estimates from four different techniques are summarized in Table 1. Our preferred mean energy estimate is in the range of 400-600 kt. Details of the analysis procedures and measurements are given in the Supplementary Information.

To establish the nature and source height of the airblast which produced damage in Chelyabinsk, we used the known trajectory[10] and a suite of videos (see Supplementary Table 5) which recorded both the fireball and the main airblast arrival, to compute acoustic travel times from each point on the fireball trajectory to each video location using a propagation model including winds developed for earlier fireball infrasound analyses[11]. The results show that the first blast wave (which also produced the damage) arrived from different altitudes at different sites, consistent with a cylindrical shock from the extended airburst, as opposed to a more point-like explosion as shown in Figure 2b. The timing residuals between observed and expected arrivals follow the bolide trail size consistent with the shock being strong early in its

propagation. The airwave reaching the city of Chelyabinsk was generated between 24 - 30 km altitude, roughly from the peak to the end of the main airburst.

In Figure 2a we show overpressure predictions from standard airblast relations based on nuclear explosions[7] as used by most impact effects models[4,6,12]. For comparison, the predictions of cylindrical line source blast theory applied to meteor entry[13] are also shown. The airblast overpressure in Chelyabinsk from window breakage measurements is 3.2±0.6 kPa (see Supplemental information for details). Noteworthy is the overestimation of overpressure using the nuclear blast relations[7]; an effect others have suggested in connection with airbursts[4]. Given that nuclear explosions release half their energy as radiation[7], thus reducing effective yield in terms of air blast energy, the nuclear curve in Figure 2a most appropriate to Chelyabinsk is ~1 Mt.

To examine if a fragmentation model[14] is consistent with the observed data and estimated object size we have applied an entry code based on a progressive fragmentation model of the initial object. Assuming an initial meteoroid of 19m diameter and a tensile strength at first fragmentation of 0.7 MPa[10] with ablation ending at ~27 km when most of the energy has been lost, we find a reasonable match to both the lightcurve and early dynamics. The final main fragmentations in this model occur near 4 MPa, very similar to those observed (1-5 MPa) in the most severe fragmentation portion of the airburst[10]. The dynamics and light production from the model are not be realistic near the terminal phase of the airburst as the model assumes all fragments split identically at each fragmentation epoch. This contradicts observations at the end of the airburst where, there is observed to be one leading fragment[10] (as opposed to dozens of identically sized individuals).

To further define the nature of the shock, we have employed the CTH simulation framework used for Tunguska[19] and comparable impactors[1] to the Chelyabinsk airburst. The simulation used all the observed trajectory parameters[10] and the observed energy as a function of height (Figure 1a.) to mimic the entry process by creating an instantaneous energy release in a sequence of momentum-preserving air cylinders along the fireball path, scaled such that the total integrated energy is 500 kt. Figure 2c and 2d shows the result of this simulation and comparison to a video record of the cloud at a similar time. The notable characteristics are that the primary shock is entirely cylindrical in contrast to point-source energy release fireball models[4,5,6] which have a strong spherical shock component. Rayleigh-Taylor instabilities that result from fast rising buoyant air in the simulation produce similar structure to that seen in videos of the dust cloud. Model overpressures for central Chelyabinsk are found to be 3 kPa, consistent with observations.

Using our best estimate for the Chelyabinsk airburst energy of ~500 kt we have estimated the bolide flux at Earth over the period 1994 - mid-2013. This estimate is based on 20 years of total global coverage by US Government or infrasound sensors, more than doubling earlier time coverage[15,16]. All events with estimated yields in excess of 1 kt are included. Figure 3 shows that this bolide flux at small sizes (<5 m diameter) is in agreement within uncertainties with telescopic[8] data and earlier infrasonic[17] influx estimates. However, at larger diameters (15m-30m), both the bolide and infrasound[17] flux curves show an order of magnitude larger apparent impact rate at Earth as compared to either telescopic surveys or the longer term average impact rate provided by lunar cratering. In both cases these inflections are due to single large events, so caution must be exercised due to small number statistics. A best fit regression line to the bolide flux is given by $N=aE^{-b}$ , where N is the cumulative number of objects with energy E (in kt) or larger impacting the Earth per year, a=3.31±0.11 and b=-

0.68±0.06. Note the exclusion of the rightmost two points (representing Chelyabinsk and two other events larger than 30 kt) produces a nearly identical slope.

Using the telescopic impact frequency[8] (green squares in Figure 3) as a baseline for the 20 year period of the bolide survey, we expect an airburst as large or larger than Chelyabinsk at the ~13% level. The independent 14 year survey by infrasound[17] (1960-1974) detected a probable 1.5 Mt airburst on Aug 3, 1963. Such a large event would be expected at the ~3% level during such a survey period. Though these deviations may be attributable to small number statistics, we note that Tunguska, with a source energy of order 3-15 Mt[18,19] (shown as a horizontal line in Figure 3) is also an extreme outlier (expected at the 2-10% level to have occurred in the last century). These events, taken together with Chelyabinsk, are increasingly suggestive of a non-equilibrium in the impactor flux for ~10-50m NEAs. This is manifested as a change in the power-law energy-frequency distribution at these sizes, similar to changes in the power-law at other sizes[20]. This is also consistent with the recent origin of Chelyabinsk as a single near-Earth asteroid and possible link to asteroid 86039[10]. Our findings support earlier interpretations of an influx maximum at this size range[21,22]. We note that telescopic surveys have only discovered ~500 NEAs of 10-20 m in size[8] (comparable to Chelyabinsk) of an estimated NEA population[23] of $\sim 2\times10^7$, implying that a non-equilibrium impactor population at these sizes could be present but not yet apparent in the discovered NEA population.

References

[1] Boslough, M. B. & Crawford, D. A. Low-altitude airbursts and the impact threat. *International Journal of Impact Engineering* **35**, 1441–1448 (2007).

[2]Harris, A. W. What Spaceguard did. *Nature* **453**, 1178–1179 (2008).

[3] Chapman, C. R. & Morrison, D. Impacts on the Earth by asteroids and comets: assessing the hazard. *Nature* **367**, 33–40 (1994).

[4] Collins, G. S., Melosh, H. J. & Marcus, R. A. Earth Impact Effects Program: A Web-based computer program for calculating the regional environmental consequences of a meteoroid impact on Earth. *Meteorit. Planet. Sci.* **40**, 817–840 (2005).

[5] Chyba, C. F., Thomas, P. J. & Zahnle, K. J. The 1908 Tunguska explosion: atmospheric disruption of a stony asteroid. *Nature* **361**, 40–44 (1993).

[6] Hills, J.G. & Goda, M.P. The fragmentation of small asteroids in the atmosphere. *Astron. J.* **105,** 1114–1144 (1993)

[7] Glasstone, S. & Dolan, P. J. *The Effects of nuclear weapons*. 3rd ed. U.S. Gov. Print Off. Washington, D.C. (1977).

[8] A. Harris, The value of enhanced NEO surveys, Planetary Defence Conference, IAA-PDC13-05-09, (2013).

[9] Werner, S.C., Harris, A.W., Neukum, G. and Ivanov, B.A. NOTE: The Near-Earth Asteroid Size-Frequency Distribution: A Snapshot of the Lunar Impactor Size-Frequency Distribution, *Icarus*, **156**, 287-290 (2002).

[10] Borovička *et al*. The entry of a small asteroid into the atmosphere over Chelyabinsk on February 15, 2013 *Nature*, this issue [11]Brown, P. G. *et al.* Analysis of a crater-forming meteorite impact in Peru. *Journal of Geophysical Research* **113**, 1–13 (2008).

[12] Toon, O. B., Zahnle, K. J., Morrison, D., Turco, R. P. & Covey, C. Environmental perturbations caused by the impacts of asteroids and comets. *Reviews of Geophysics* **35**, 41–78 (1997).

[13] Revelle, D. O. On meteor-generated infrasound. *Journal of Geophysical Research* **81**, 1217–1230 (1976).Reed, J. W. & Pape, B. Evaluation of window pane damage intensity in San Antonio resulting from Medina Facility explosion on November 13, 1963. *Annals of the New York Academy of Science* **52**, 565–584 (1968).

[14] ReVelle, D. O. NEO fireball diversity: energetics-based entry modeling and analysis techniques in *Proceedings of the International Astronomical Union Symposium No. 236: NEOs, our Celestial Neighbors: Opportunity and Risk* **2**, 95–106 (2007).

[15] Brown, P. G., Spalding, R. E., ReVelle, D. O., Tagliaferri, E. & Worden, S. P. The flux of small near-Earth objects colliding with the Earth. *Nature* **420**, 294–296 (2002).

[16] Ens, T. A., Brown, P. G., Edwards, W. N. & Silber, E. Infrasound production by bolides: A global statistical study. *Journal of Atmospheric and Solar-Terrestrial Physics* **80**, 208–229 (2012).

[17] Silber, E., ReVelle, D. O., Brown, P. G. & Edwards, W. N. An estimate of the terrestrial influx of large meteoroids from infrasonic measurements. *Journal of Geophysical Research* **114**, 1–8 (2009).

[18] Ben-Menahem, A., Source parameters of the Siberian explosion of June 30, 1908, from analysis and synthesis of seismic signals at four stations, *Physics of the Earth and Planetary Interiors*, **11**, 1-35 (1975)

[19] Boslough, M. B. & Crawford, D. Shoemaker-Levy 9 and Plume-forming Collisions on Earth. *Annals of the New York Academy of Science,* **822,** 236–282 (1997).

[20] Bland, P. A. & Artemieva, N. The rate of small impacts on Earth. *Meteoritics & Planetary Science* **41**, 607–631 (2006).

[21] Ceplecha, Z. Influx of interplanetary bodies onto Earth. *Astronomy and Astrophysics* **263**, 361–366 (1992).

[22] Ward, S. & Asphaug, E. Asteroid Impact Tsunami: A Probabilistic Hazard Assessment. *Icarus* **145,** 64–78 (2000).

[23] Data from http://ssd.jpl.nasa.gov accessed on June 22, 2013.

[24] Brachet, N. et al., Monitoring the Earth's Atmosphere with the Global IMS Infrasound Network in *Infrasound monitoring for atmospheric studies*. (Pichon, A. Le, Blanc, E. & Hauchecorne eds) pp. 77-118 (Springer Dordrecht Heidelberg London New York: 2010).

[25] Brown, P. G. *et al.* The fall of the Grimsby meteorite-I: Fireball dynamics and orbit from radar, video, and infrasound records. *Meteoritics & Planetary Science* **363**, 339–363 (2011).

[26] Borovička, J. et al. The Košice meteorite fall: Atmospheric trajectory, fragmentation, and orbit. *Meteoritics & Planetary Science,* doi: 10.1111/maps.12078 (2013)

[27] Tagliaferri, E., Spalding, R., Jacobs, C., Worden, S.P., and A. Erlich, Detection of Meteoroid Impacts by Optical Sensors in Earth Orbit, in *Hazards due to Comets and Asteroids* (ed Gehrels, T.) pp. 199-221 (Univ. Arizona Press, Tucson, 1994)

**Supplementary Information** is available in the online version of the paper at www.nature.com/nature.

**Acknowledgements** Funding provided by NASA co-operative agreement NNX11AB76A and Czech institutional project RVO:67985815. DPD acknowledges support from the Office of Naval Research. We appreciate discussions with Freeman Gilbert (UCSD), Jeff Stevens (SAIC), Paul Earle and John Bellini (USGS). D. Dearborn provided assistance with video reductions.

**Author Contributions** P.G.B, N.B, D.B., L.C., W.E., L.E., M.G., A.L., J.A., P.M., P.S., and R.W. performed various aspects of the identification, measurement and interpretation of infrasound records. L.A., C.D.H., M.H., G.L. collected and identified the airburst signals in seismic recordings as well as analysed and interpreted the seismic data. P.G.B. R.B., J.B., W.C., J.G., A.K., D.M., R.W., A.S., P.S. helped in identifying important videos and their geolocation and various aspects of their measurements. M.B and M.C.B. performed bolide entry modeling. D.D. provided atmospheric model data and interpretation. Z.K., J.G. and R.J.W. performed video lightcurve analysis and calibrations and helped with their interpretation as well as measurements of video dust cloud features. R.E.S and E.T. facilitated and interpreted US Government Sensor data. D.U. performed window breakage analysis. P.G.B. and E.S. performed analysis of acoustic propagation and associated computer code development. P.G.B wrote the manuscript. All authors commented on the manuscript.

**Author Information** Reprints and permissions information is available at www.nature.com/reprints. The authors declare no competing financial interests. Correspondence and requests for materials should be addressed to P.B. (pbrown@uwo.ca).

**TABLE 1 Airburst energy estimates for the Chelyabinsk fireball from multiple technologies**.

| Technique | Best Estimate [kt] | Range [kt] |
|---|---|---|
| Seismic | 430 | 220 - 630 |
| Infrasound (Mean Period) | 600 | 350 - 990 |
| US Government Sensor | 530 | 450 - 640 |
| Video-derived lightcurve | >470 | |

Here kt refers to kilotons TNT equivalent energy (=$4.185\times10^{12}$ J). To estimate the energy from infrasonic airwaves, all 42 infrasound stations of the International Monitoring System[24] were examined. Of these, 20 stations showed clear signals from the airburst. Our infrasound energy estimates are based on the average observed dominant infrasound period from one dozen stations having stratospheric returns showing the highest signal-to-noise ratio. Seismic Rayleigh waves generated by the fireball shock wave impinging on the Earth's surface just south of Chelyabinsk were detected by ~70 seismic stations at ranges in excess of 4000km. The amplitude of these waves in specific passbands as calibrated to nuclear airbursts[18] were used as an independent estimate of source energy.

**Figure Captions**

**FIGURE. 1 Lightcurve of the Chelyabinsk Airburst.**

**a.** The brightness profile for the Chelyabinsk fireball based on indirect illumination measured from video records. The brightness is an average derived from indirect scattered sky brightness from six videos proximal to the airburst, corrected for the sensor gamma setting, autogain, range and airmass extinction following the procedure used for other fireball lightcurves generated from video[25,26]. The lightcurve has been normalized based on the US Government sensor data peak brightness value of $2.7\times10^{13}$ W/sr, corresponding to an absolute astronomical magnitude of -28 in the silicon bandpass. The individual video lightcurves deviate by less than one magnitude between times -2,+1.5 with larger deviations outside this interval. Time zero corresponds to 03:20:32.2 UTC, Feb 15, 2013

**b.**The energy deposition per unit height for the Chelyabinsk airburst based on video data. The conversion to absolute energy deposition per unit path length assumes a 6000K blackbody emission and 17% bolometric efficiency following the assumptions used to convert earlier US Government sensor information to energy[27]. The heights are computed using the calibrated trajectory[10] and common features on lightcurves between video sites, resulting in a height accuracy of ~1 km. The total energy of the airburst found by integrating under the curve is > 470 kt. The half energy deposition height range is 33-27 km; these are the heights at which energy deposition falls below half the peak value of ~ 80 kt/km (height), which is reached near 29.5 km altitude.

**FIGURE. 2. Observed and predicted shock characteristics for the Chelyabinsk fireball.**

**a.** Theoretical airblast overpressures using standard nuclear weapons relations[7] and cylindrical-line source blast theory[13] appropriate to central Chelyabinsk. The nuclear relation

curves (in black) assume a spherical point source at a specific height. Shown are assumed yields of 500 kt (dashed line) and 1 Mt (dotted line). The cylindrical-line source blast model (red line) uses the energy deposition per unit length from Figure 1b to define an equivalent blast radius as the source and assumes that the shock is linear at the ground.

**b**. Shows travel time residuals between the time of fireball passage at each height and the main airwave arrival for 38 videos (see Supplementary Table 5). The residuals show the observed arrival time (corrected for fireball motion) - expected time calculated assuming propagation at the local adiabatic sound speed and incorporating winds[11]. Shown for comparison is the width of the visible trail. This is consistent with faster than ambient sound speed travel expected for the shock-wave near the fireball. The minimum timing residuals suggest shock source heights vary between 30 -23 km across Chelyabinsk as opposed to originating from a point source.

**c.** The apparent cross section of CTH simulation 50 seconds after .5 Mt was sourced into segmented cylinder of air. Trail is colored according to temperatures. Outer shaded area reveals envelope of shocked air - note the dominant cylindrical shock. The box is 100 km wide.

**d**. Shown for comparison with c, a video frame of the dust cloud taken 250 km to the SW of the fireball path looking North (source: http://www.youtube.com/watch?v=lCv9S0Z0e0E, author: Evgeny Volkov). Approximately 140 km of the end portion of the fireball trail is shown some 40-60 sec after passage of the fireball.

**FIGURE. 3 The estimated cumulative flux of impactors at the Earth**. The bolide impactor flux at Earth (Bolide flux 1994-2013 - black circles) based on ~20 years of global observations from US Government sensors and infrasound airwave data. Global coverage averages 80% among a total of 58 observed bolides with E > 1 kt and includes the

Chelyabinsk bolide (far right black circle). This coverage correction is approximate and the bolide flux curve is likely a lower limit. The brown-coloured line represents an earlier power-law fit from a smaller dataset for bolides between 1 - 8 m in diameter[15]. Error bars represent counting statistics only. For comparison, we plot de-biased estimates of the near-Earth asteroid impact frequency based on all asteroid survey telescopic search data through mid-2012 (green squares)[8] and other earlier independently analysed telescopic datasets[15] including NEAT discoveries (pink squares) and finally from the Spacewatch (blue squares) survey, where diameters are determined assuming an albedo of 0.1. Energy for telescopic data is computed assuming a mean bulk density of 3000 $kgm^{-3}$ and average impact velocity of 20.3 $kms^{-1}$. The intrinsic impact frequency for these telescopic data was found using an average probability of impact for NEAs as $2\times10^{-9}$ per year for the entire population. Lunar crater counts converted to equivalent impactor flux and assuming a geometric albedo of 0.25 (grey solid line) are shown for comparison[9], though we note that contamination by secondary craters and modern estimates of the NEA population which suggest lower albedos will tend to shift this curve to the right and down. Finally, we show estimated influx from global airwave measurements conducted from 1960-1974 which detected larger (5-20m) bolide impactors (upward red triangles)[17] using an improved method for energy estimation compared to earlier interpretations of these same data.

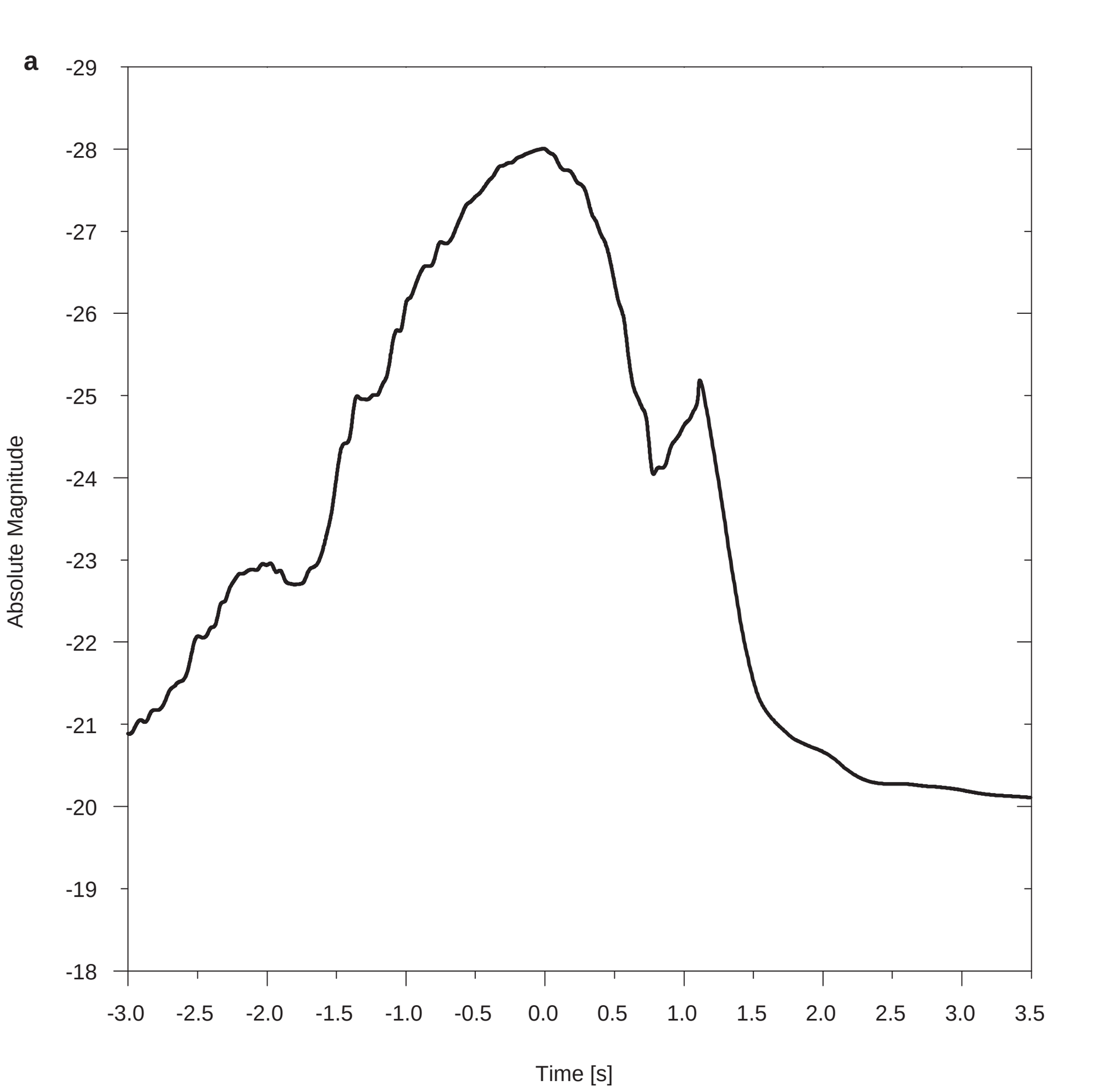
a
-29
-28
-27
-26
-25
-24
-23
-22
-21
-20
-19
-18
Absolute Magnitude
-3.0
-2.5
-2.0
-1.5
-1.0
-0.5
0.0
0.5
1.0
1.5
2.0
2.5
3.0
3.5
Time [s]

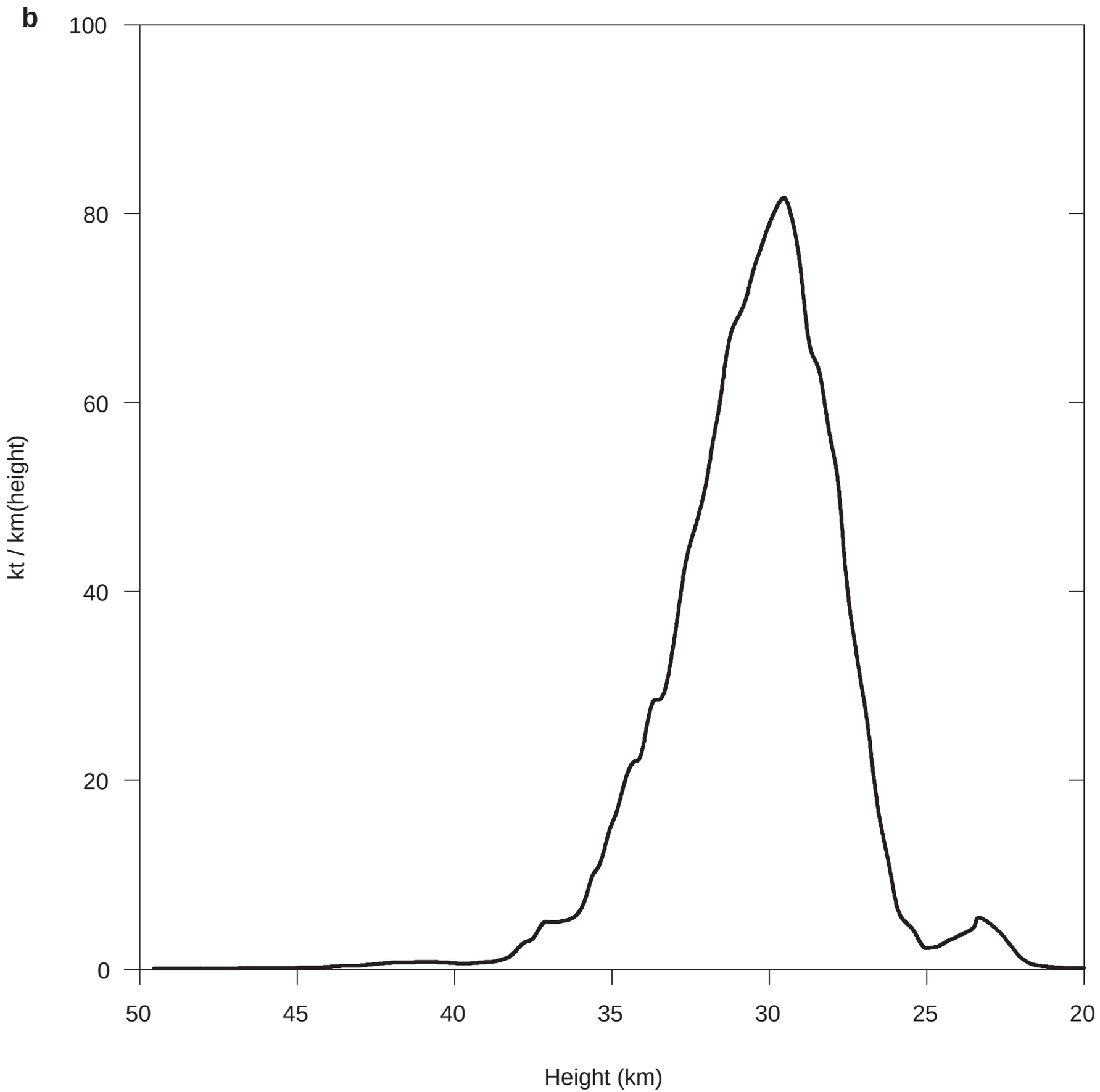
b
100
80
60
40
20
0
kt / km(height)
50
45
40
35
30
25
20
Height (km)

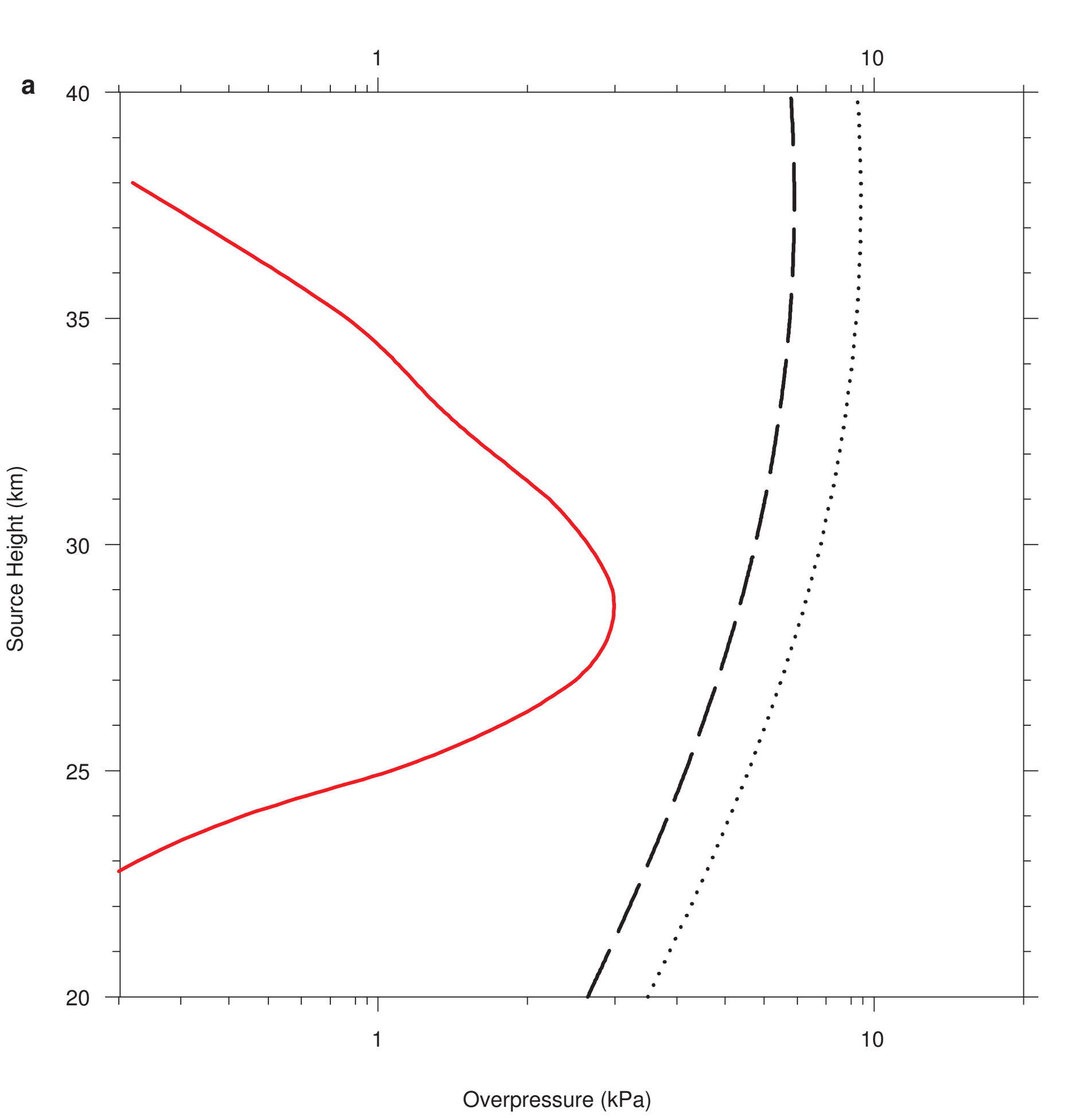
a
1
10
40
35
30
25
20
Source Height (km)
1
10
Overpressure (kPa)

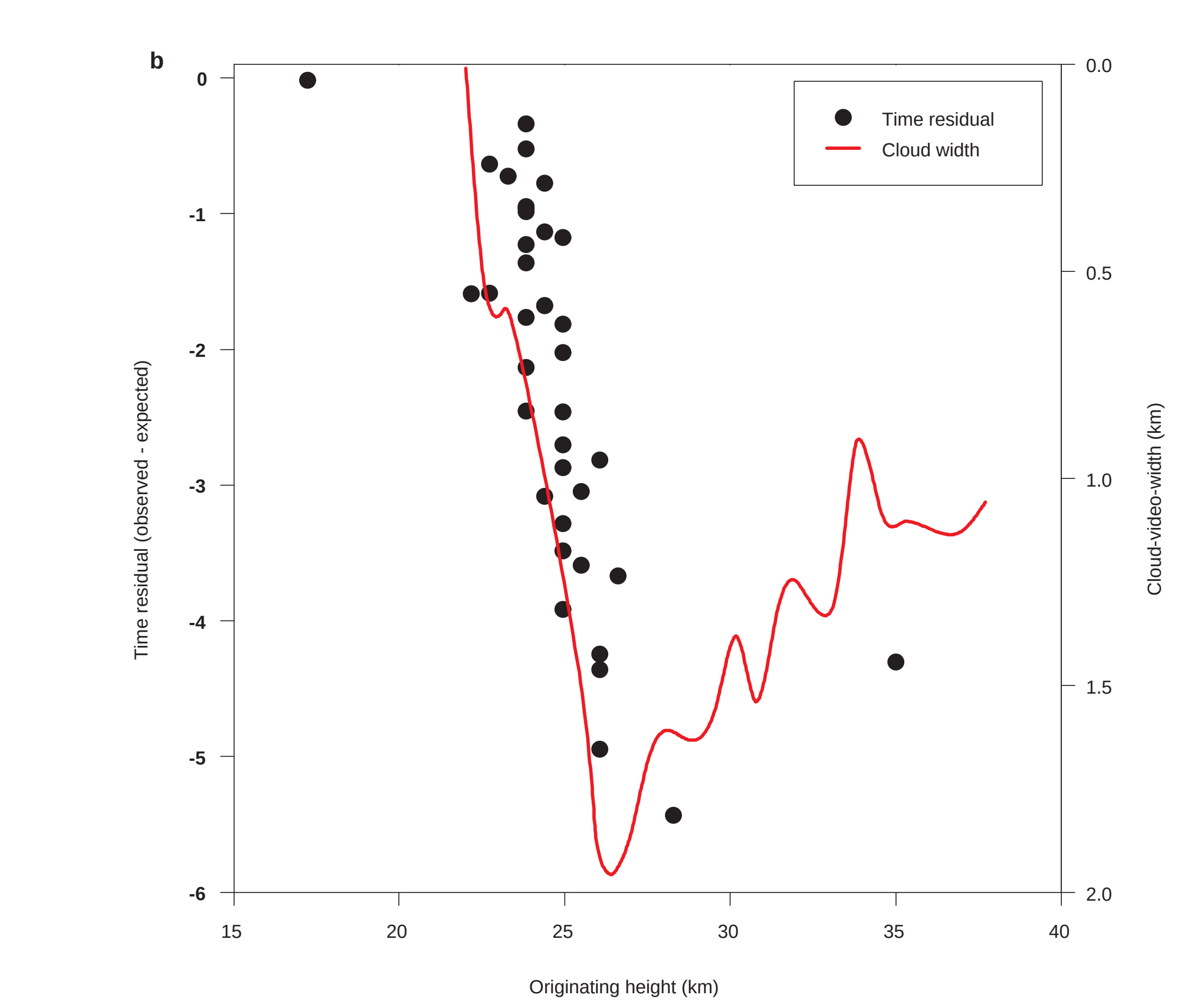
b
Time residual
Cloud width
Time residual (observed - expected)
Cloud-video-width (km)
Originating height (km)
0
-1
-2
-3
-4
-5
-6
0.0
0.5
1.0
1.5
2.0
15
20
25
30
35
40

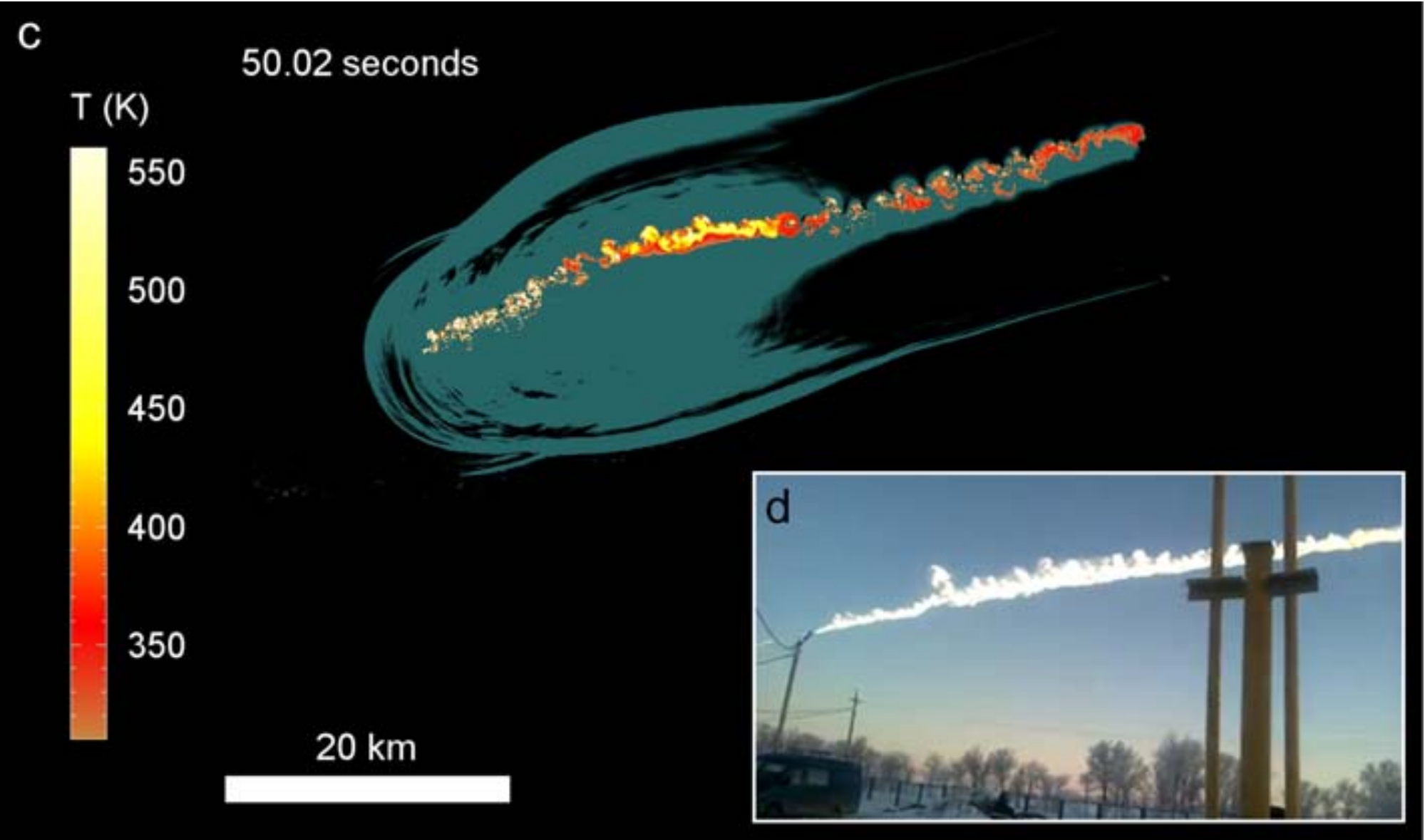
c
50.02 seconds
T (K)
550
500
450
400
350
20 km
d

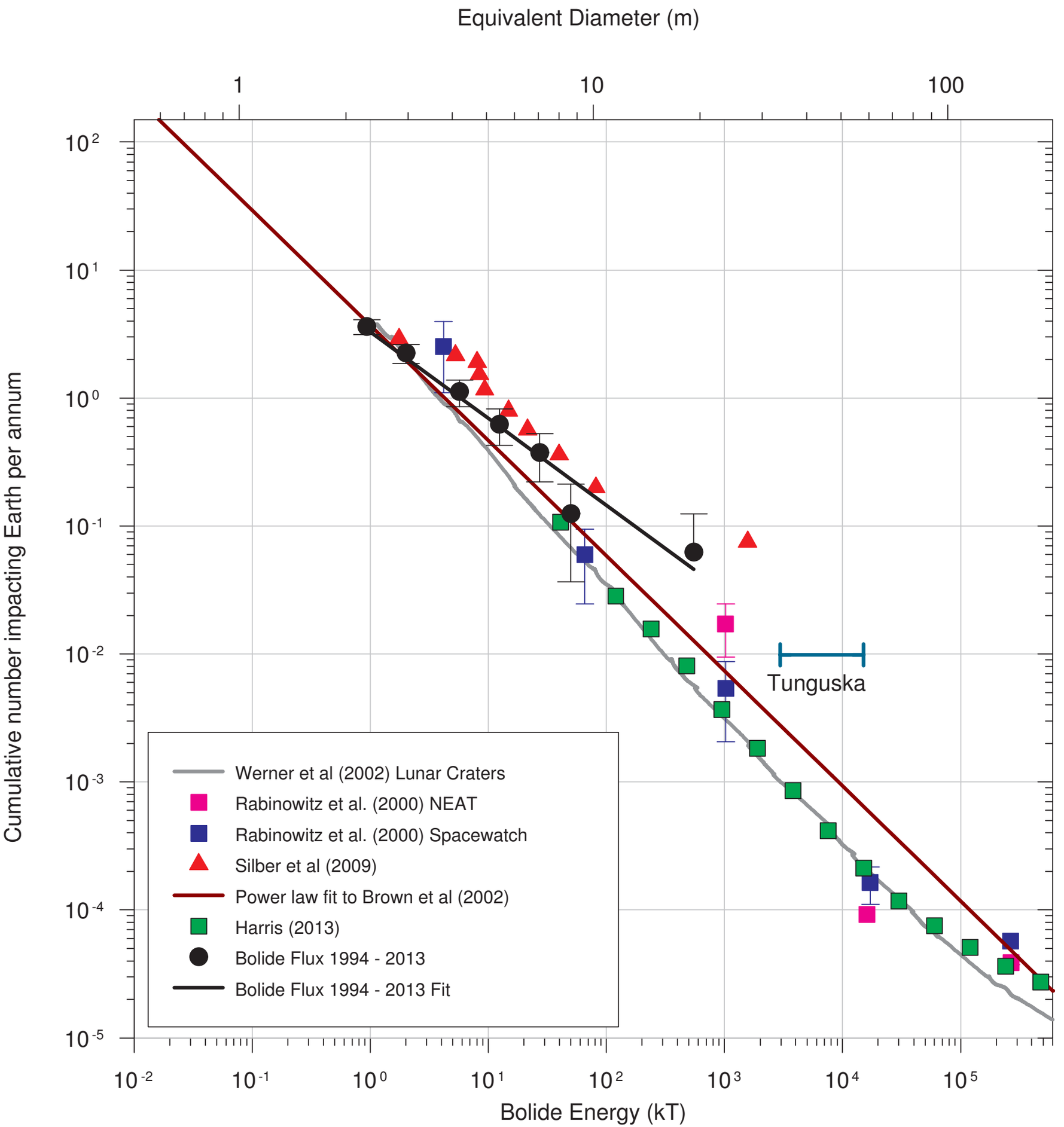
Equivalent Diameter (m)
1
10
100
Cumulative number impacting Earth per annum
$10^{2}$
$10^{1}$
$10^{0}$
$10^{-1}$
$10^{-2}$
$10^{-3}$
$10^{-4}$
$10^{-5}$
$10^{-2}$
$10^{-1}$
$10^{0}$
$10^{1}$
$10^{2}$
$10^{3}$
$10^{4}$
$10^{5}$
Bolide Energy (kT)
Tunguska
Werner et al (2002) Lunar Craters
Rabinowitz et al. (2000) NEAT
Rabinowitz et al. (2000) Spacewatch
Silber et al (2009)
Power law fit to Brown et al (2002)
Harris (2013)
Bolide Flux 1994 - 2013
Bolide Flux 1994 - 2013 Fit